2023 IEEE/RSJ International Conference on Intelligent Robots and Systems (IROS)
October 1-5, 2023. Detroit, USA

Design, Characterization and Control of a Whole-body Grasping and Perching (WHOPPEr) Drone

Weijia Tao, Karishma Patnaik, Fuchen Chen, Yogesh Kumar and Wenlong Zhang*

***Abstract*— Flying robots can exploit perching abilities to position themselves on strategically-chosen locations and monitor the areas of interest from a critical vantage point. Moreover, they can significantly extend their battery life by turning off the propulsion systems when carrying out a surveillance mission. However, unknown disturbances arise from the physical interactions between the robot and the object, making it challenging to stabilize the robot during perching. In this paper, we present a Whole-body Grasping and Perching (WHOPPEr) Drone, which is capable of fast and robust perching by utilizing its entire body as the grasper in lieu of an add-on grasper. We first present the design concept, parameter selection and characterization of the novel whole-body grasping drone. Next, we analyze the grasping ability of the morphing chassis and present an aerodynamic analysis for the effect of motor thrust on the compliant arm. We finally demonstrate, via real-time experiments, the performance of WHOPPEr in autonomous perching and payload delivery tasks.**

I. Introduction

Nature has always inspired researchers to design flying robots that can mimic their avian counterparts [1]. It is incredible how birds can effectively leverage their bodies and navigate through narrow spaces, and perform high-speed grasping and perching on irregular objects. With constant efforts to obtain these agile flying characteristics, researchers have started endowing conventional multirotor drones with various abilities such as folding, perching, and grasping towards various ends [2]–[5]. Perching, in particular, has many applications that can be exploited by flying robots to maintain a critical surveillance position and conserve energy. However, a perching maneuver involves physical interactions with the target object and is prone to impact forces, making it critical to design a compliant and robust grasper for various sizes of the perching target for mission success.

There are generally two ways to achieve perching with a drone: one is to add a grasper on a drone, and the other one is to use its own body as the grasper. For the first case, researchers have designed compliant graspers to mitigate impact-induced disturbances [4], [6], [7]. Soft bodies can withstand significantly higher interaction forces and can conform to irregular objects, making them excellent candidates for interaction-rich tasks. A soft aerial robot designed specifically for aerial manipulation tasks reported high success rates in the presence of interaction forces [8]. However, this grasper was not validated for perching missions where the entire weight of the drone has to be accounted for by the grasper instead of relying on the motor thrust. Conventionally, custom-designed and add-on grasping mechanisms are employed for perching, which adds extra weight, reduces battery life, and limits the mission success to perches with certain sizes and shapes [9]–[11]. The grippers proposed for nano and micro-aerial vehicles can seldom be scaled up for use in mini-drones because of the light-weight materials used to design the grasper which cannot hold the weight of the larger drones [12], [13]. Other perching mechanisms based off tethered cables, gecko-inspired designs and micro-spines constrain the flying space and the target location [14]–[16]. More recently, perching mechanisms have been developed that harvest impact energy for activation and ensure secure perching [17]–[19]. All these drones, however, try to address the problem of perching by attaching additional grasping mechanisms to the main body. In addition to the extra weights, these grasping mechanisms require the drone to be precisely controlled so that the perching target falls within the (oftentimes limited) work space of the grasper.

For the second case, the drone arms are utilized as grasper fingers instead of adding a subsystem for grasping. A whole-body grasping drone was commercialized as a flyable and wearable micro-drone (motor-motor distance less than 150mm) [20] with limited autonomy. Mini-drones with a compliant body, on the contrary, are tricky to design, owing to the large thrust ranges that they operate in, which can

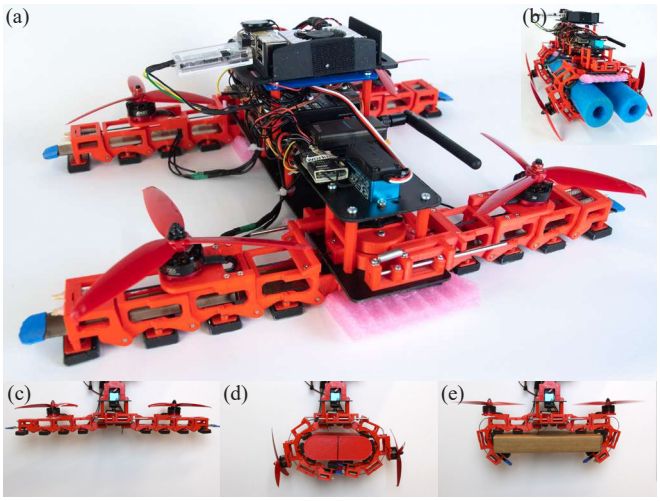

Fig. 1. (a) A novel drone, WHOPPEr, that can perch and grasp. (b) The drone in the perching configuration. (c) Flying demo. (d) Perching demo. (e) Grasping demo.

The authors are with The School of Manufacturing Systems and Networks, Ira A. Fulton Schools of Engineering, Arizona State University, Mesa, AZ, 85212, USA. Email: {wtao11, kpatnaik, fchen65, ykumar6, wenlong.zhang}@asu.edu.
* Address all correspondence to this author.

2023 IEEE/RSJ International Conference on Intelligent Robots and Systems (IROS) | 978-1-6654-9190-7/23/$31.00 ©2023 IEEE | DOI: 10.1109/IROS55552.2023.10341722

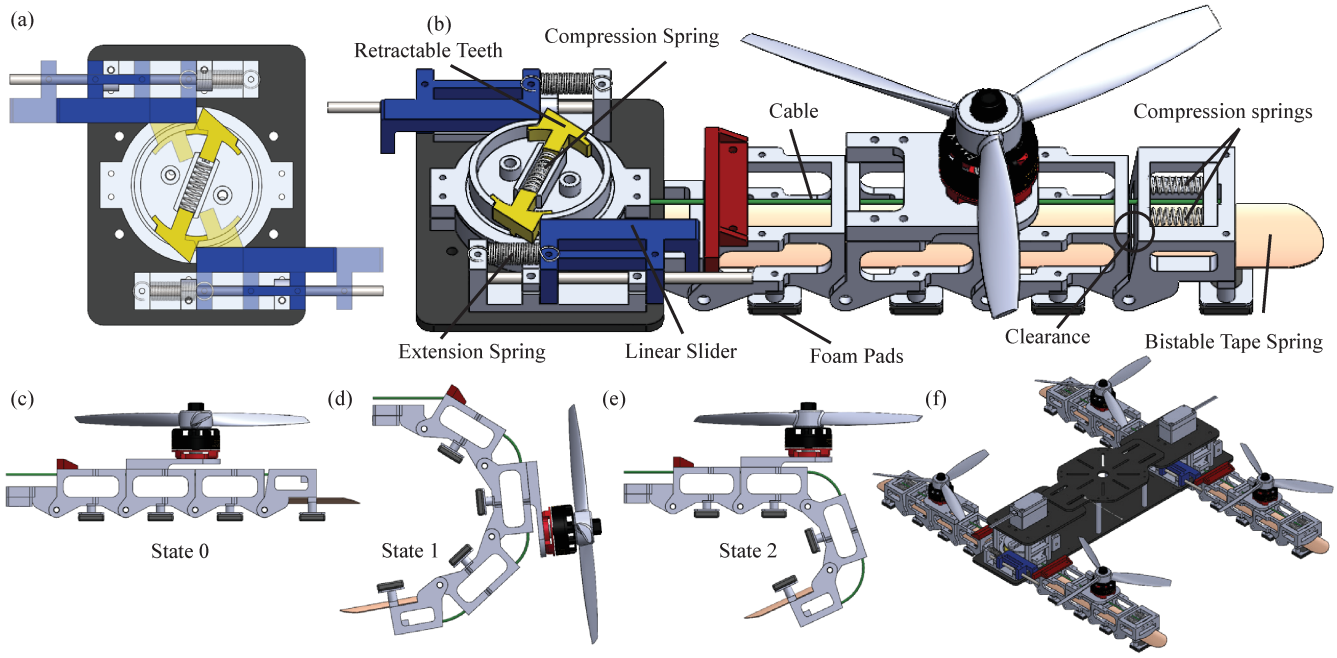

Fig. 2. (a) Motion of a ratchet-like gear system. (b) Arm design and actuation mechanism. (c) State 0: Normal state. (d) State 1: Engaged state. (e) State 2: Partially retracted state. (f) The assembled drone

destabilize the drone by introducing undesired aerodynamic effects on the flexible arms. Thanks to the significant advancements in flexible and foldable drone research [21], mini-drones (motor-motor distance between 150mm and 600mm) have also recently been shown to perform perching [22]. Such designs, however, have limitations on the shape of the perch objects to ensure a successful perch, akin to the issues with rigid graspers. Another whole-body perching drone [23] was recently proposed for perching and employs a bistable mechanism to engage the arms. However, all these designs do not demonstrate the capabilities of the drone for grasping an object and flying back, such as for payload delivery, therefore only solving perching ability and not pushing the boundaries for other applications.

Our proposed concept involves the utilization of 1) the whole body for perching, which reduces the added weight and increases the grasp workspace, and 2) partial body engagement for grasping objects. To the best of the authors' knowledge, this is the first time a multirotor drone demonstrates autonomous whole-body perching and payload delivery without sacrificing controllability. It should be noted that this work employs an active perching mechanism, unlike impact-based passive perching, to attempt perching from different angles. To realize this concept, the drone incorporates a bistable structure inside its arms, which has been shown to enhance efficiency and stability in previous studies [18], [19], [23]. Furthermore, our drone features a unique mechanism that utilizes servos to trigger and recover the bistable arms for perching, and propeller thrust to partially retract the arm for grasping while maintaining altitude stabilization. Overall, this proposed mini-drone, WHOPPEr, shown in Fig. 1, has a motor-to-motor distance is 358mm and weighs approximately 1.6kg, including all the electronics and batteries. The drone is capable of achieving a maximum grasping force of around 40N, allowing for a robust grasp even in the presence of environmental disturbances.

The remainder of the paper is organized as follows. In Section II, we present the design and manufacturing process of WHOPPEr. In Section III, we characterize the grasper properties of the WHOPPEr body and perform experiments to study the arm deflection. In Section IV, we describe the multirotor dynamics and control of WHOPPEr for a perching and grasping task, and present the complete control framework. Finally, Section V describes the results of real-time experiments for an indoor perching task, and Section VI concludes the article and discusses future directions.

II. Design and Fabrication

The functional requirements for the drone include the ability to perch using its entire body and grasp objects with a portion of its body, with no energy consumption required during perching or grasping. Additionally, the drone should be capable of switching between different configurations and rejecting disturbances caused by the environment.

A. Arm Design

The drone arm is a crucial element of the design, with three distinct states, as shown in Figs. 2(c)-(e). In State 0, the arm is in its normal position and remains straight, providing stability during flight. During State 1, the arm is fully coiled and engaged, enabling the drone to perch on objects of varying geometries. In State 2, the arm is partially retracted, allowing for conventional drone hovering, with the coiled tip of the arm still capable of transporting objects during flight.

The drone arm design features a multi-link structure capable of bending and recovering in response to external forces (Fig. 2(b)). The arm is comprised of five 3D-printed links connected via metal pins, with a bistable tape spring located at the bottom of the arm providing gripping force. To optimize the arm's conformability with different objects, multiple links were incorporated, but too many links sacrifice the rigidity of the arm. In addition, a physically locked structure was implemented with the links to prevent twisting and ensure one-direction bending.

A bistable tape spring was employed due to its ability to generate gripping force, which is commonly used in products such as slap bracelets. To achieve a larger grasping force, the arm contains three layers of tape springs, which is the maximum number that the actuator can activate. Each link of the arm contains a slot that allows the tape spring to slide and buckle. As shown in Fig. 2(b), there is a clearance to allow the arm to slightly deflect upward when the cable is pulled and the curvature of the tape spring is fixed at the tip, which are both desired to unbuckle the tape spring as determined by experiments. Foam pads with friction tapes are also incorporated with the arm to enhance gripping strength.

B. Actuation Mechanism

To achieve a smooth transition between the three states, a specially designed actuation mechanism is implemented in Fig. 2(a). This mechanism integrates several key components, including a ratchet-like center gear with spring-loaded retractable teeth, a spring-loaded linear slider, and a cable-driven system, as shown in Fig. 2(b). The linear slider is used to trigger the arm to the engaged State 1 (Fig. 2(d)), while the cable-driven system can retract the arm back to its normal State 0 (Fig. 2(c)). Additionally, the motor and propeller thrust can bring the arm to a partially retracted State 2 (Fig. 2(e)). The cables connect all the arm links and are fastened to a pulley under center gear, and are adjustable by a nob underneath. Since two arms share the center pulley and servo in the final drone, compression springs are connected to the cables to make sure both arms can be fully retracted even if their cable lengths are slightly different (Fig. 2(b)). A servo is used to drive the center gear, and a motor with a propeller is mounted on the arm to provide thrust.

As shown in Figs. 2(a) and 2(b), with a counterclockwise rotation of the gear, the cable is released, and the teeth on the gear push the linear slider outward, producing a torque on the arm that triggers its movement to the engaged state. Once the movement is complete, the spring-loaded slider automatically returns to its initial position to prevent impediment to the link's motion when the motor thrust partially retracts the arm. The motor is mounted on the middle link of the arm, enabling the remaining links of the arm to be utilized as an effective grasper for holding an object. With a clockwise rotation, the cable retracts, the teeth on the gear are pushed back by the sliders, and the arm is backed to its normal state. The ratchet-like retractable teeth prevent the sliders from moving outward during this process (Fig. 2(a)). As a result, there is no conflicting motion when the arm is retracted by the cable. This mechanism also can drive the arm directly from the engaged State 1 to the normal State 0 when needed.

C. Drone Assembly

To construct the drone in Fig. 2(f), we attach two arms to a central gear and actuate them synchronously. The frame of the drone consists of a fiberglass plate, which is both lightweight and highly durable. Two pairs of arms are mounted onto this plate. In addition, a power distribution board and a layer of fiberglass are incorporated into the frame to securely attach all the necessary servos and electronics. The space between the layers and the top of the drone accommodates all the electronics, such as the flight controller batteries. The drone uses the Pixhawk4 (Auterion, Zürich, Switzerland) commercial flight controller with an UPBoard (Intel Co. California, United States) as the high-level companion computer. Four brushless DC motors, Emax RS2205, with 6-inch propellers (Gemfan Flash 6042, Gemfanhobby Co. Ltd, Ningbo, China) are used for drone control generation. Two high-torque servo motors (DS3235SG270 35KG, Annimos, Shenzhen, China) are used for the arm activation. It also uses two BECs (ICE-20A-SB, GARTT, Shenzhen, China) to separately power the high-level companion computer at 5V and the servo motors for the arm activation at 7.4V. The drone's motor-to-motor distance measures 358mm, and it is equipped with a Lipo battery (2200mAh 50C 4S, Zeee Power Co. Ltd, Shenzhen, China). Overall, the drone has an approximate weight of 1.6kg.

III. System Characterization

In this section, we describe the grasping and structure characterization of WHOPPEr for various scenarios.

A. Grasping Characterization

A set of static pulling experiments as shown in Fig. 3(a) was carried out to better understand the grasping force of the proposed arm design. Two shapes are selected for the objects to grasp: a rectangular box and a rectangular box with rounded edges. The width of the objects is always 140mm and the height is one of 30mm, 50mm, and 70mm. Therefore, there are a total of six different objects and three trials are performed for each object. The experiment is done utilizing a universal tensile testing machine (UTM) (Instron 5944, Instron Corp., High Wycombe, United Kingdom). For each trial, a pair of arms and the object is first mounted on the UTM. The distance between the object and the foam pads of the arms is set to 5mm. After the arm is triggered by its servo and wraps around the object, the UTM pulls the object straight away from the arm at a speed of 1mm/s until the arms completely lose contact with the object or the force exceeds 30N to avoid damaging the device. The elapsed time, displacement, and force exerted on the object are recorded at 10Hz. In post-processing, the force data are filtered with a second-order Butterworth low-pass filter with a cutoff frequency of 0.05Hz to remove the fluctuations caused by small slippage and noise from the buckling of the tape springs. The arm is considered to lose its grasp if

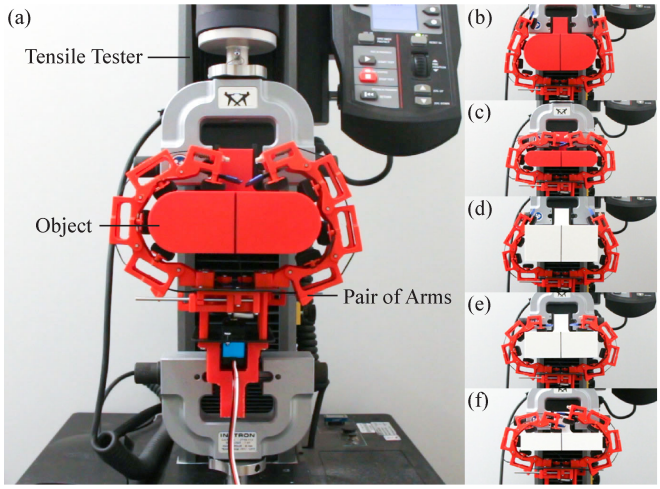

Fig. 3. (a) The grasper characterization experiment setup and the grasper holding rounded rectangular objects with (b) 70mm, (a) 50mm, and (c) 30mm height and rectangular objects with (d) 70mm, (e) 50mm, and (f) 30mm height. The widths of the objects are 140mm.

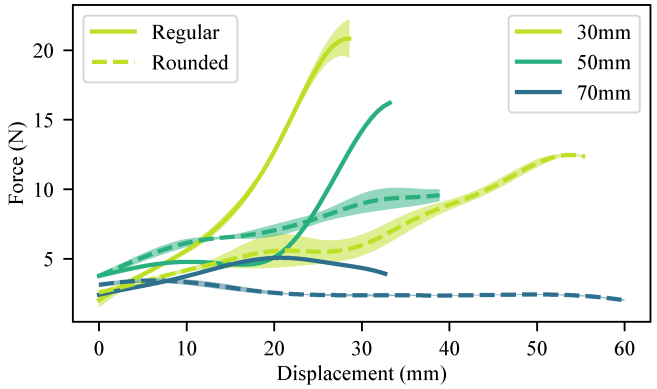

Fig. 4. The grasping force vs displacement with different object shapes.

there is a sudden big slippage, which roughly correlates to a decrease in the force of 0.2N for the last 1mm based on examinations of the experiment footage and data.

As shown from the results plotted in Fig. 4, the pair of arms perform better when grasping rectangular boxes without rounded edges and reaches a maximum grasping force of over 20N[1] for the one with 30mm height. This is likely due to the 90-degree corners getting caught into the gaps between the foam pads as shown in Fig. 3(d), which does not happen for the rounded edges as shown in Fig. 3. On the other hand, the more evenly distributed contact force between the arms and the rounded objects delays slippage, extending the holding range up to 60mm for the rounded object with 70mm height. Another trend is that as the height of the object increases, the grasping force decreases because the arms fail to fully wrap around the object.

B. Structure Characterization

As mentioned in Section IIA, final paragraph, a minimum deflection of at least 10mm in the direction of the positive

[1]The entire drone uses two pairs of arms and therefore can achieve a maximum of 40N in theory.

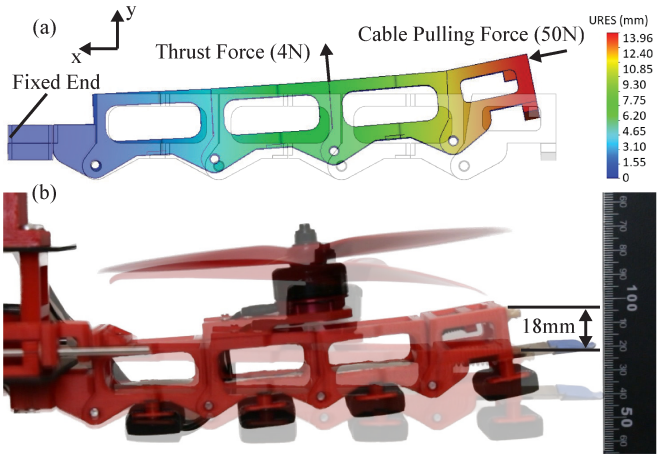

Fig. 5. Deflection of the arm under loading condition: thrust force (4N) and cable pulling force (50N). (a) Simulation results show a maximum deflection of 13.96 mm. (b) A maximum deflection of 18 mm is observed during the experiment.

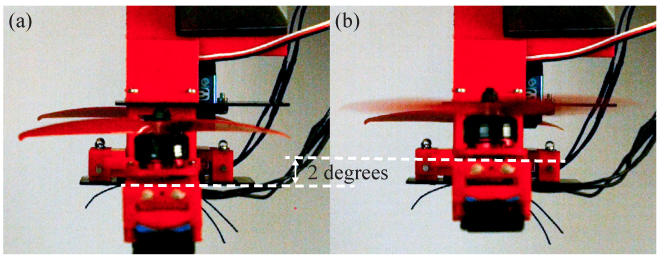

Fig. 6. Torsional deflection between (a) zero and (b) full throttle

y-axis (Fig. 5) is desired to unbuckle the bistable tape spring used in the arm to switch from State 1 or 2 to State 0 as shown in Fig. 2. To assess the arm design, static stress analysis using appropriate material, fixtures, and connections is done using the SolidWorks simulation tool as shown in Fig. 5(a). The simulation results show a maximum deflection of 13.96mm under the thrust force (4N) in the positive y-axis, and the cable pulling force (50N) in the positive x-axis direction. The experimental results under the same loading condition showed a deflection of 18mm as shown in Fig. 5(b).

For evaluating the effects on aerodynamics due to any torsional characteristics of the drone arm, we employ a high-speed camera at 500fps (Edgetronics SC1, CA, USA) to record the experiment and use this data to visually calculate the angular deflection due to torsional moment. These values come to about 2 degrees as shown in Fig. 6. Furthermore, we infer that since the structure is symmetrical, the aerodynamic losses due to bending, shown in Fig. 5(b), are minor and the drone retains normal flight albeit with some aerodynamic losses.

IV. Control of WHOPPEr

A. Modeling and Control

In this section, we present the robust adaptive controller for WHOPPEr to perform successful perching and payload delivery missions.

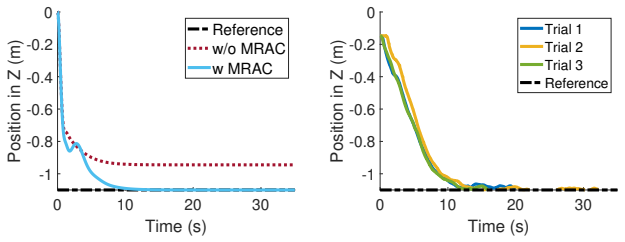

(a) Simulations (b) Experimental Results

Fig. 7. Comparison of the tracking performance in z direction at hover conditions for the adaptive flight controller. (a) Without the adaptive controller, the gains have to be adjusted and tuned for various payloads, however with MRAC, even with incorrect initial mass assumption, one can see the tracking performance is improved due to the mass parameter adaptation. (b) the z trajectory tracking performance during experiments.

Let $\boldsymbol{x} \in \mathbb{R}^3, \boldsymbol{v} \in \mathbb{R}^3$ denote the position and velocity of WHOPPEr in the world frame. Then, if $R \in \mathbb{R}^{3\times3}$ denotes the orientation of the system in the world frame and $\Omega \in \mathbb{R}^3$ denotes the body-frame angular velocity, we can express the dynamics of WHOPPEr as

$$\dot{\boldsymbol{x}} = \boldsymbol{v}, m\dot{\boldsymbol{v}} = mge_3 - fRe_3 \tag{1a}$$

$$\dot{R} = R\hat{\Omega}, J\dot{\Omega} - [J\Omega]_\times \Omega = \tau + \delta \tag{1b}$$

where m denotes the unknown mass of the entire drone, $[f\ \tau]^T$ denote the control inputs of thrust, $f \in \mathbb{R}$ and torques $\tau \in \mathbb{R}^3$ respectively and $J \in \mathbb{R}^{3\times3}$ denotes the moment of inertia.

The controller is modified from a conventional geometric controller on $\mathsf{SE}(3)$ [24] to account for the change in mass due to different payloads. In this work, we implemented a model reference adaptive controller (MRAC) for the translational dynamics to improve the tracking performance of WHOPPEr for adaptive payloads. Specifically, the MRAC is employed to estimate the mass whenever there is an additional payload since this unaccounted mass addition adversely affects the z-direction trajectory. We choose MRAC since the translational dynamics of WHOPPEr have a known form of a second-order system and the control specifications can be neatly specified in the form of the desired response. We choose the dynamics of this reference plant, $\ddot{x}_m(t)$, as the following:

$$\ddot{x}_m + \lambda_1 \dot{x}_m + \lambda_2 x_m = \lambda_2 x_d(t) \tag{2}$$

with the reference model output $x_m \in \mathbb{R}$ being the ideal mass parameter. We tuned parameters $\lambda_1 = 2, \lambda_2 = 5$ to follow the desired reference $x_d(t)$. The control thrust f is then generated according to:

$$f = -(-k_x e_x - k_v e_v - \hat{m}ge_3 + \hat{m}\ddot{x}_d) \cdot Re_3 \tag{3a}$$

$$\dot{\hat{m}} = -\gamma\nu s \tag{3b}$$

$$s = \dot{\tilde{x}} + \lambda\tilde{x} \tag{3c}$$

$$\nu = \ddot{x}_m - 2\lambda\dot{\tilde{x}} - \lambda^2\tilde{x} \tag{3d}$$

where $\tilde{x}(t) := x(t) - x_m(t)$. This is similar to the conventional thrust generation techniques for drones, but with the adjustable parameter $\hat{m}$. Since the quantity m in (1) is not known exactly, therefore an estimate of m, $\hat{m}$, is obtained from the proposed parameter estimator law (3b)-(3d). This value of $\hat{m}$ is then employed to generate the required f. We choose $\gamma = 0.5$ and $\lambda = 1$ to achieve a critically damped response for trajectory tracking in the z-direction.

Furthermore, the change in the vehicle's inertia vector is modeled as fixed inertia with bounded uncertainty such that $\|\delta\| \leq \Delta$. A robust controller is accordingly implemented in the attitude loop to address the modeling uncertainty as proposed in [25] with $\Delta = 0.01$ as the bound on uncertainty.

Simulation results and comparison with experiments for a hover test are shown in Fig. 7. For the simulation, we initialize the tracking maneuver with an initial mass estimate $\hat{m}(0)$ = 1.5kg while the actual mass m = 1.7kg. We see that without MRAC, there is a steady state error in the tracking performance as seen in Fig. 7(a). This adaptive controller is implemented on the flight control unit and overall, the 3D tracking error has a root-mean-square error (RMSE) of 2.83cm for real experiments as shown by the consistent tracking performance for three trials in Fig. 7(b).

V. Experimental Results

As discussed in Section IIC, we use the commercial off-the-shelf flight controller Pixhawk4 with an UPBoard as the high-level companion computer for all our experiments. The complete closed-loop control architecture is shown in Fig. 8. We use ROS2 to communicate between the high-level companion computer and the flight controller via an RTPS bridge. In this section we demonstrate the experimental results with WHOPPEr in two case scenarios - (i) an indoor perching and recovery task and (ii) a payload delivery task. All the experiments are conducted in an indoor drone studio at ASU using a motion capture system (OptiTrack, NaturalPoint Inc, OR) for obtaining the localization data and 3D pose estimation of the drone.

A. Perching and Recovery

The perching strategy is implemented as described in Fig. 8. The screenshots from the experimental demonstration are shown in Fig. 9(a) and the corresponding z-trajectory plot is shown in Fig. 9(b). Individual markings depict each distinct state of the entire perching and recovery maneuver. First, the drone takes off, shown by marking (1), reaches a desired hover target location (2), and then initiates a vertical descent toward the target object. After a set time duration, the servos are used to activate the arms to perch as shown by marking (3) and go to State 1. Note that the wait time to engage the servo is tuned after multiple trials to be around 2 seconds.

Next, after a user-specified wait time, the drone initiates the recovery and returns to the home maneuver. The propeller thrust is sufficient to release the grasp and bring the arms to a plane such that motors are upright, as discussed in Section II. This State 2 is marked by (4) after which the drone then tries to hover at a specified location with the arms partially engaged as shown by marking (5).

Finally, we employ the servo to completely retract the arms, shown by markings (6) and (7) to go to State 0, and

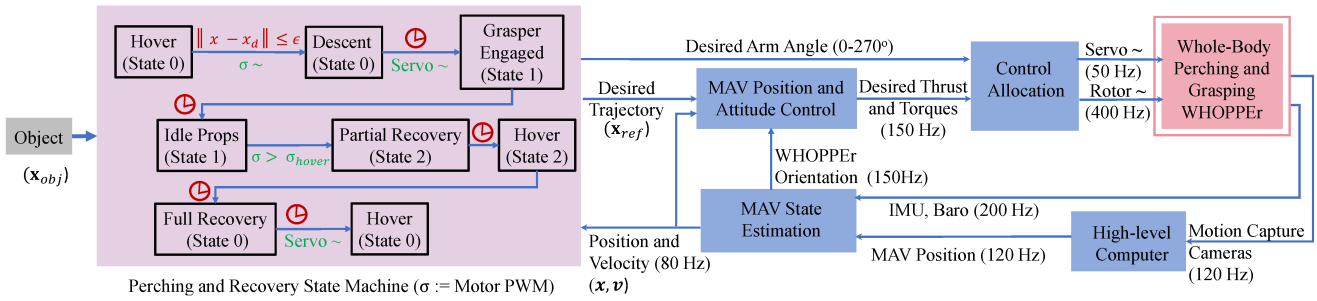

Fig. 8. The complete autonomous perching, recovery, and retrieval control framework. We use an indoor motion capture system to get the localization data for the 3D pose estimation of the drone. The red-colored labels depict user-defined wait times or condition-triggered events. The green colored words beside each arrow show the actuation signal to obtain the next State. Finally, the hover and descent blocks show the transition sub-trajectories employed to meet each State's desired initial condition.

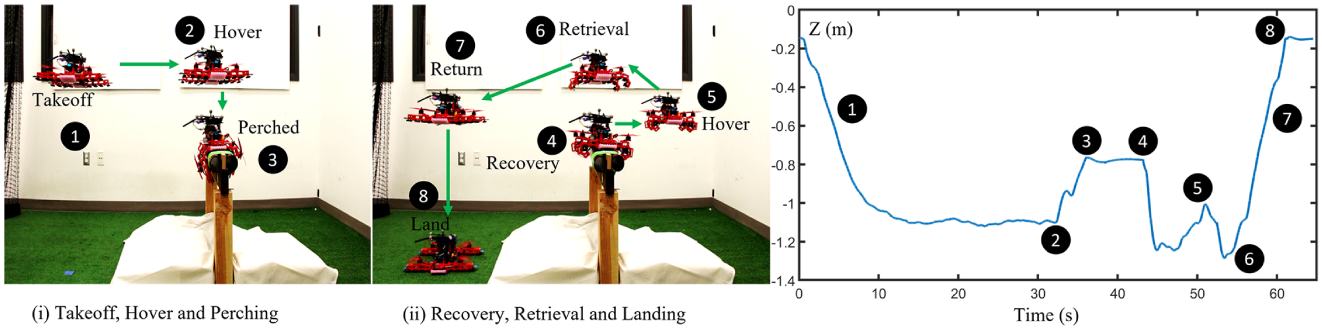

(i) Takeoff, Hover and Perching (ii) Recovery, Retrieval and Landing

(a) Screenshots from Experimental Demonstration

(b) Z Trajectory during the Maneuver

Fig. 9. (a) Autonomous perching, recovery, and retrieval demonstration in experiments. (b) Z trajectory during the entire perching and recovery maneuver. The maneuver consists of the following continuous maneuvers - the drone first approaches the target (1), hovers (2), and perches on the object (3). After a specific wait time, it initiates recovery to State 2, shown by marker (4), retrieves its arms (6)-(7), and lands at the desired location (8).

land at the home position, marking (8). We also see that the performance of the controller is not affected by the arm engaging and disengaging process, as shown by the tracking performance before and after the perching. However, during the arm retrieval in positions labeled by (5)-(7), while in hover, there is a slight height loss due to the disturbance introduced by the retrieval mechanism shown by marking (5) in Fig. 9. This height loss is quickly recovered and the drone flies back to the home position for landing. We repeat this perching experiment multiple times and it is seen that since the controller is not robust to the ground effect, there is a drift of position while landing, leading to a land success rate of 60%. However, once the drone lands stably, it has a 100% perching success rate.

B. Payload Delivery

We also demonstrate the capabilities of the proposed drone for an autonomous delivery task as shown in Fig. 10(a), also presented in the Supplementary Video. The drone's arms are used as graspers to hold a rectangular object of dimension 35cm×20cm×2cm, weighing 80g, and deliver at a specified target location. In Fig. 10, (1) shows the marking where the payload is placed below the drone. The arm-based grasper is then engaged, marking (2), and the drone flies off with the payload, shown by marking (3) to deliver the load at the home position, marking (4). The adaptive controller accounts for any change in mass and inertia as shown by the successful payload delivery experiments.

C. Angled Perch and Disturbance

We also demonstrate that the drone can perform angled perching at an angle of 65 degrees from the horizontal reference line and when subject to manually induced disturbances, it resists the disturbance and maintains a robust perch as shown in Figs. 10(b) and (c).

VI. Conclusion

In this paper, we presented a novel multirotor drone, WHOPPEr, which could perform whole-body grasping for perching maneuvers. We showed how this drone could withstand the impacts and disturbances during perching and yielded a robust perching maneuver. Also, the proposed perching mechanism was fast and able to conform to objects of various sizes. The characterization shows that our drone is able to provide a maximum grasping force of 40N, which contributes to successful perching. The proposed design not only helps in robust perching but can also be used for camouflaging during pursuit applications. In addition to perching, we further demonstrated the possibility of grasping objects with this morphology and extended our design for pick-and-place missions. Furthermore, the proposed MRAC framework for the flight controller generates consistently

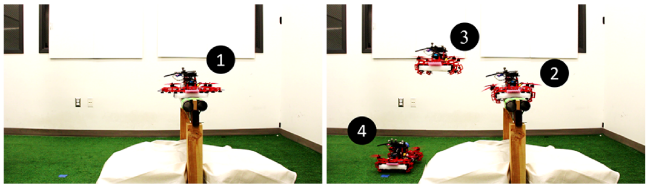

(a) Payload Placed Under, Grasping, Hover and Landing

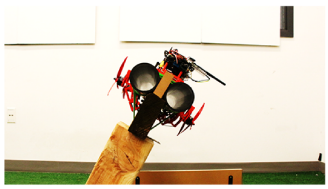

(b) An Angled Perch

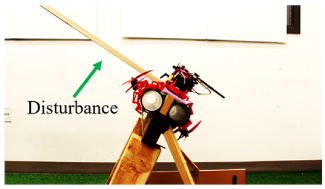

(c) Angled Perch Subject to Disturbance

Fig. 10. (a) Screenshots from an experimental demonstration for an autonomous delivery task. (1) shows the object placed under the drone to facilitate grasping, (2) shows the grasped state, (3) shows the flying back after grasping the object and (4) shows the drone landing at a given location to deliver the object. (b) Demonstrates an angled perching configuration (c) The angled perch is manually disturbed by applying forces and shows the robustness of the perch, also shown by the Supplementary Video.

good tracking performance for adaptive payloads and leads to successful autonomous perching, grasping, and recovery maneuvers.

For future work, we would like to conduct more thorough experiments about the drone including the payload size and weight limits in State 2, flight time and maneuverability with or without payload, more grasping and perching scenarios, and comparisons with other state-of-the-art implementations. Furthermore, we will work on performing physics-based simulations to completely characterize the arms as graspers, for optimizing the design and further reducing its weight. In addition, we would like to employ computer vision in the autonomous flight controller to detect strategic perch locations outdoors and attempt perching, evaluating the performance of the overall system in more realistic settings. The ground effect encountered during the approach to the target will be modeled and compensated by the flight controller to perform aggressive perching maneuvers.

Acknowledgement

The authors would like to thank Dr. Pham Huy Nguyen for the initial brainstorming and Prof. Daniel Aukes for sharing equipment for building the drone.

References

[1] S. Mintchev and D. Floreano, "Adaptive morphology: A design principle for multimodal and multifunctional robots," *IEEE Robotics & Automation Magazine*, vol. 23, no. 3, pp. 42–54, 2016.

[2] K. Patnaik, S. Mishra, S. M. R. Sorkhabadi, and W. Zhang, "Design and control of SQUEEZE: A Spring-augmented QUadrotor for intEractions with the Environment to squeeZE-and-fly," in *IEEE/RSJ International Conference on Intelligent Robots and Systems*, pp. 1364–1370, IEEE, 2020.

[3] W. R. Roderick, M. R. Cutkosky, and D. Lentink, "Touchdown to take-off: at the interface of flight and surface locomotion," *Interface focus*, vol. 7, no. 1, p. 20160094, 2017.

[4] S. Mishra, D. Yang, C. Thalman, P. Polygerinos, and W. Zhang, "Design and control of a hexacopter with soft grasper for autonomous object detection and grasping," in *Dynamic Systems and Control Conference*, vol. 51913, p. V003T36A003, American Society of Mechanical Engineers, 2018.

[5] S. Mishra and W. Zhang, "A disturbance observer approach with online q-filter tuning for position control of quadcopters," in *American Control Conference*, pp. 3593–3598, IEEE, 2017.

[6] A. McLaren, Z. Fitzgerald, G. Gao, and M. Liarokapis, "A passive closing, tendon driven, adaptive robot hand for ultra-fast, aerial grasping and perching," in *IEEE/RSJ International Conference on Intelligent Robots and Systems*, pp. 5602–5607, IEEE, 2019.

[7] K. A. Hoffmann, T. G. Chen, M. R. Cutkosky, and D. Lentink, "Bird-inspired robotics principles as a framework for developing smart aerospace materials," *Journal of Composite Materials*, p. 00219983231152663, 2023.

[8] J. Fishman, S. Ubellacker, N. Hughes, and L. Carlone, "Aggressive grasping with a "soft" drone: From theory to practice," in *IEEE/RSJ International Conference on Intelligent Robots and Systems*, 2021.

[9] C. E. Doyle, J. J. Bird, T. A. Isom, J. C. Kallman, D. F. Bareiss, D. J. Dunlop, R. J. King, J. J. Abbott, and M. A. Minor, "An avian-inspired passive mechanism for quadrotor perching," *IEEE/ASME Transactions On Mechatronics*, vol. 18, no. 2, pp. 506–517, 2012.

[10] K. Hang, X. Lyu, H. Song, J. A. Stork, A. M. Dollar, D. Kragic, and F. Zhang, "Perching and resting—a paradigm for uav maneuvering with modularized landing gears," *Science Robotics*, vol. 4, no. 28, 2019.

[11] S. Kirchgeorg and S. Mintchev, "Hedgehog: Drone perching on tree branches with high-friction origami spines," *IEEE Robotics and Automation Letters*, 2021.

[12] H. Zhang, *Biologically Inspired Perching for Aerial Robots*. PhD thesis, Colorado State University, 2021.

[13] A. Braithwaite, T. Alhinai, M. Haas-Heger, E. McFarlane, and M. Kovač, "Tensile web construction and perching with nano aerial vehicles," in *Robotics research*, pp. 71–88, Springer, 2018.

[14] H.-N. Nguyen, R. Siddall, B. Stephens, A. Navarro-Rubio, and M. Kovač, "A passively adaptive microspine grapple for robust, controllable perching," in *2019 2nd IEEE International Conference on Soft Robotics (RoboSoft)*, pp. 80–87, IEEE, 2019.

[15] J. Thomas, G. Loianno, M. Pope, E. W. Hawkes, M. A. Estrada, H. Jiang, M. R. Cutkosky, and V. Kumar, "Planning and control of aggressive maneuvers for perching on inclined and vertical surfaces," in *International Design Engineering Technical Conferences and Computers and Information in Engineering Conference*, vol. 57144, p. V05CT08A012, American Society of Mechanical Engineers, 2015.

[16] H. Lee, C. M. Harris, A. P. Payan, and D. Mavris, "Risk-aware trajectory planning using energy-based analysis for aerial vehicles," in *AIAA Aviation Forum*, p. 3175, 2021.

[17] M. Kovač, J. Germann, C. Hürzeler, R. Y. Siegwart, and D. Floreano, "A perching mechanism for micro aerial vehicles," *Journal of Micro-Nano Mechatronics*, vol. 5, no. 3, pp. 77–91, 2009.

[18] W. Roderick, M. Cutkosky, and D. Lentink, "Bird-inspired dynamic grasping and perching in arboreal environments," *Science Robotics*, vol. 6, no. 61, p. eabj7562, 2021.

[19] P. H. Nguyen, K. Patnaik, S. Mishra, P. Polygerinos, and W. Zhang, "A Soft-Bodied Aerial Robot for Collision Resilience and Contact-Reactive Perching," *Soft Robotics*, Apr. 2023.

[20] "Nixie - the first wearable camera that can fly." `https://www.youtube.com/watch?v=kfzqUsGMHE0&ab_channel=FlyNixie`. Last Accessed: 07.30.2023.

[21] K. Patnaik and W. Zhang, "Towards reconfigurable and flexible multi-rotors," *International Journal of Intelligent Robotics and Applications*, vol. 5, no. 3, pp. 365–380, 2021.

[22] N. Bucki, J. Tang, and M. W. Mueller, "Design and control of a midair-reconfigurable quadcopter using unactuated hinges," *IEEE Transactions on Robotics*, vol. 39, no. 1, pp. 539–557, 2022.

[23] P. Zheng, F. Xiao, P. H. Nguyen, A. Farinha, and M. Kovac, "Metamorphic aerial robot capable of mid-air shape morphing for rapid perching," *Scientific Reports*, vol. 13, no. 1, p. 1297, 2023.

[24] T. Lee, M. Leok, and N. H. McClamroch, "Geometric tracking control of a quadrotor uav on se (3)," in *49th IEEE conference on decision and control*, pp. 5420–5425, IEEE, 2010.

[25] K. Patnaik and W. Zhang, "Adaptive Attitude Control for Foldable Quadrotors," *IEEE Control Systems Letters*, vol. 7, pp. 1291–1296, 2023.